Computers and Fluids 176 (2018) 260–265

Contents lists available at ScienceDirect

Computers and Fluids

journal homepage: www.elsevier.com/locate/compfluid

Turbulent drag reduction in channel flow with viscosity stratified fluids

Somayeh Ahmadi [a,b], Alessio Roccon [a,b], Francesco Zonta [a,b], Alfredo Soldati [a,b,c,*]

[a] *Institute of Fluid Mechanics and Heat Transfer, TU Wien, Austria*
[b] *Dipartimento Politecnico di Ingegneria e Architettura, Universitá di Udine, Italy*
[c] *Department of Fluid Mechanics, CISM, 33100, Udine, Italy*

ARTICLE INFO

Article history:
Received 21 April 2016
Revised 11 November 2016
Accepted 15 November 2016
Available online 25 November 2016

Keywords:
Viscosity stratification
Turbulence
Direct numerical simulation
Phase field method

ABSTRACT

In this work we use Direct Numerical Simulation (DNS) to study the turbulent Poiseuille flow of two immiscible liquid layers inside a rectangular channel. A thin liquid layer (fluid 1) flows on top of a thick liquid layer (fluid 2), such that their thickness ratio is $h_1/h_2 = 1/9$. The two liquid layers have the same density but different viscosities (viscosity-stratified fluids). In particular, we consider three different values of the viscosity ratio $\lambda = \nu_1/\nu_2$: $\lambda = 1$, $\lambda = 0.875$ and $\lambda = 0.75$. Numerical Simulations are based on a Phase Field method to describe the interaction between the two liquid layers. Although a small viscosity ratio is assumed, this physical setup aims at mimicking the situation where water (less viscous fluid) is used to favour the transport of oil (large viscous fluid) inside pipelines. Compared with the case of a single phase flow, the presence of a liquid-liquid interface produces a remarkable turbulence modulation inside the channel, since a significant proportion of the kinetic energy is subtracted from the mean flow and converted into work to deform the interface. This induces a strong turbulence reduction in the proximity of the interface and causes a substantial increase of the volume-flowrate. These effects become more pronounced with decreasing λ.

1. Introduction

Confined flows of cocurrent immiscible fluids are often observed in the process and petroleum industry. Important examples include oil-water separators and hydrocarbon transportation pipelines. In these situations, two-immiscible phases (typically oil and water) are driven inside pipelines/channels and interact modifying the overall mass, momentum and heat transfer properties of the system. To optimize the design of these systems it is crucial to determine whether the two phases remain separate (due to density and viscosity stratification) or form emulsions (which are difficult to process/separate). From a practical standpoint, the stratified condition (or even the core annular flow condition) is preferred for two main reasons: the required power to transfer the oil/water flow is lower (due to the lower viscosity of water wetting a wall compared to that of the oil) and oil can be easily separated from water (whereas more complex oil/water separators must be designed when water is dispersed within the oil phase).

When a base state with separate phases (stratified flow) can be defined, a rigorous linear stability analysis of the governing equations [1,2] can be done to determine if the base state is stable. Note that this linear analysis can only predict whether small disturbances will grow and their nature. Nonlinear theories are instead needed to determine if wave saturation of small-waveslope waves occurs [3,4]. However, waves usually become large and form subharmonics that can interact so to produce triadic resonance. In all these cases, no theoretical prediction can be made, and experiments or accurate numerical simulations are required to capture the complex dynamics of liquid-liquid flows.

Technical challenges to obtain detailed information on the velocity/stress field in experiments of immiscible and stratified liquid-liquid flows have hindered the identification of the dominant mechanisms controlling the flow dynamics and have made difficult the development of robust physics-based wave generation models. Direct Numerical Simulation (DNS) is a useful tool for examining the detailed flow physics in such instances, in particular in the proximity of the deformed interface. For this reason, it can be used to provide important insights into the characterization of the interfacial dynamics.

In literature, there exists a number of studies focusing on the dynamics of interfacial waves in air-water two phase flows (see [5,6] and references therein). However, much less is known about

* Corresponding author. Fax: +43 (1) 5880132299.
E-mail addresses: alfredo.soldati@tuwien.ac.at, soldati@uniud.it (A. Soldati).

http://dx.doi.org/10.1016/j.compfluid.2016.11.007
0045-7930/

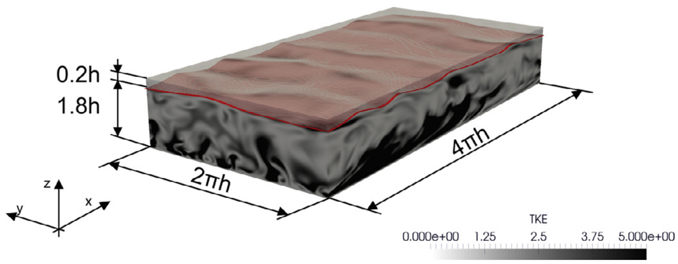

Fig. 1. Sketch of the computational domain with details of the flow configuration. A thin liquid layer with smaller viscosity (fluid 1) flows on top of a thick liquid layer with larger viscosity (fluid 2). The thickness ratio between the two liquid layers is $h_1/h_2 = 1/9$. The distribution of Turbulent Kinetic Energy (TKE) and the deformed liquid-liquid interface are also shown for visualization purposes.

the dynamics of liquid-liquid interfaces (except for a series of studies on the stability of oil-water flows, [7–11]).

In the present study, we want to use Direct Numerical Simulations (DNS) to analyze the dynamics of a turbulent viscosity-stratified liquid-liquid flow moving inside a flat channel. For the first time, a Phase Field approach (Cahn–Hilliard equation) is employed here to describe the liquid-liquid interaction in such configuration. The governing balance equations are solved through a pseudo-spectral method for a given value of the reference shear Reynolds number ($Re_\tau = 100$) and for three different values of the viscosity ratio λ between the two liquid-layers ($\lambda = 1,\ \lambda = 0.875$ and $\lambda = 0.75$).

Compared with the case of a single phase flow driven by the same pressure gradient, the viscosity stratified liquid-liquid flow is characterized by a larger volume flowrate, as a direct consequence of the conversion of mean kinetic energy into work to deform the liquid-liquid interface. These effects become stronger with increasing the viscosity difference between the two liquid layers.

2. Methodology

We consider the case of two immiscible fluid layers flowing inside a rectangular channel, with the upper part of the channel occupied by fluid 1 and the lower part of the channel occupied by fluid 2 (as sketched in Fig. 1). The interface between the two fluid is located in the upper part of the channel, and the film thickness ratio is $h_1/h_2 = 1/9$. The two fluids have the same density ($\rho_1 = \rho_2 = \rho$, i.e gravity is negligible), but different viscosities ($\nu_1 \neq \nu_2$). As a consequence, a viscosity ratio $\lambda = \nu_1/\nu_2$ can be defined. To model the mixture of two immiscible, incompressible and newtonian fluids we use a Phase Field approach. The fluid dynamics of the system is described by the following set of dimensionless equations [12–15]:

$$\nabla \cdot \mathbf{u}=\mathbf{0} \tag{1}$$

$$\frac{\partial \mathbf{u}}{\partial t} + \mathbf{u}\cdot\nabla\mathbf{u} = -\nabla\tilde{p} + \frac{1}{Re_\tau}\nabla^2\mathbf{u} + \nabla\cdot\left[k(\phi,\lambda)\left(\nabla\mathbf{u}+\nabla\mathbf{u}^{\mathbf{T}}\right)\right] + \frac{3}{\sqrt{8}}\frac{1}{WeCh}\mu\nabla\phi \tag{2}$$

$$\frac{\partial\phi}{\partial t} = -\mathbf{u}\cdot\nabla\phi + \frac{1}{Pe}\nabla^2\mu \tag{3}$$

$$\mathcal{F}(\phi) = f_0(\phi) + \frac{1}{2}Ch^2|\nabla\phi|^2 = \frac{1}{4}(\phi-1)^2(\phi+1)^2 + \frac{1}{2}Ch^2|\nabla\phi|^2 \tag{4}$$

$$\mu = \frac{\delta\mathcal{F}}{\delta\phi} = \phi^3 - \phi - Ch^2\nabla^2\phi \tag{5}$$

Eqs. (1) and (2) describe the conservation of mass (continuity) and momentum (Navier-Stokes) of the system, with $\mathbf{u} = (u_x, u_y, u_z)$ being the velocity field and $\tilde{p}$ the corrected pressure field [16]. Eq. (3) is the Cahn-Hilliard equation that describes the transport of the order parameter ϕ used to model the binary mixture: ϕ is constant in the bulk fluid regions (where $\phi = \pm 1$) and changes smoothly across the fluid-fluid interface. The free energy functional $\mathcal{F}(\phi)$ of the system (Eq. (4)), is the sum of two different contribution: a double-well potential $f_0(\phi)$ that accounts for the phobic behavior of the phases and a non-local term that accounts for the effect of surface tension ($\propto|\nabla\phi|^2$). The variation of the free energy functional is called chemical potential μ and controls the behavior of the interfacial layer (Eq. (5)). Note that Eqs. (2) and (3) are coupled through the capillary term $\frac{3}{\sqrt{8}}\frac{1}{WeCh}\mu\nabla\phi$ that describes the momentum exchange between the two phases across the interface.

The term $k(\phi, \lambda)$ in Eq. (2) is introduced to account for the non-uniform viscosity of the system. Viscosity can be written as a linear function of the order parameter ϕ [17,18]

$$\nu(\phi) = \nu_1\frac{1+\phi}{2} + \nu_2\frac{1-\phi}{2}. \tag{6}$$

Introducing the viscosity ratio λ, the viscosity field can be written as the sum of a uniform and a non-uniform part as [19,20]:

$$\nu(\phi,\lambda) = \nu_2 + \nu_2(\lambda-1)\frac{(\phi+1)}{2}. \tag{7}$$

In dimensionless units, the non uniform part of the viscosity field becomes

$$k(\phi,\lambda) = \frac{1}{Re_\tau}(\lambda-1)\frac{(\phi+1)}{2}. \tag{8}$$

The following dimensionless groups appear in Eqs. (1)–(5):

$$Re_\tau = \frac{u_\tau h}{\nu_2} \qquad Pe = \frac{u_\tau h}{\mathcal{M}} \qquad We = \frac{\rho u_\tau^2 h}{\sigma} \qquad Ch = \frac{\xi}{h}, \tag{9}$$

where σ is the surface tension of the liquid-liquid interface, $\mathcal{M}$ is the mobility, and ξ the thickness of the liquid-liquid interface within the PF method. The reference length of the problem is the half channel height h, whereas the reference velocity is the shear velocity $u_\tau = \sqrt{\tau_w/\rho}$, with τ_w the shear stress at the wall defined in terms of the viscosity of the thicker liquid layer ν_2. The physical meaning of the dimensionless groups is the following. The Reynolds number (Re_τ) is the ratio between the inertial and the viscous forces (defined based on the viscosity ν_2). The Weber number (We) is the ratio between the inertial and the surface tension forces. Small values of We represent a rigid interface, whereas large values of We represent an highly deformable interface. The Peclet number (Pe) is the ratio between the convective and the diffusive time-scale, and it quantifies the relaxation time of the interface. The larger is Pe, the larger is the time required by the interface to adapt to the external forcing. Finally, the Cahn number (Ch) is the dimensionless thickness of the interface.

3. Numerical simulations

Governing equations (Eqs. (1)–(3)) are solved using a pseudo-spectral method based on transforming the field variables into wavenumber space through Fourier series in the homogeneous directions (x and y) and Chebyshev polynomials in the wall-normal direction (z). Integration in time is achieved using an implicit Crank-Nicolson scheme for the uniform part of the diffusive terms, and using an explicit Adams-Bashforth scheme for both the non-uniform part of the diffusive terms (in Eq. (2)) and the nonlinear terms. In particular, the nonlinear terms are first computed in the physical space and then transformed in the wavenumber space using a de-aliasing procedure based on the 2/3 rule; derivatives are evaluated directly in the wavenumber space to maintain spectral accuracy. The dimensionless value of the time step

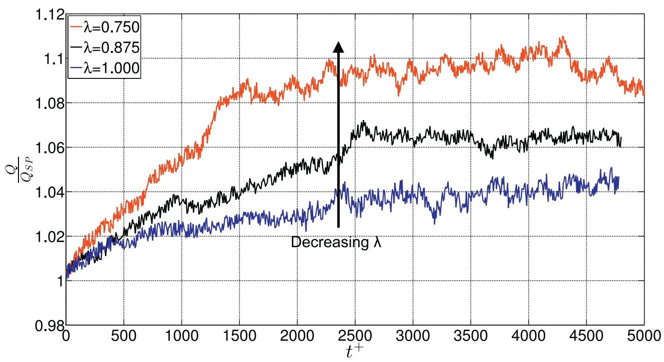

Fig. 2. Time evolution of the volume flowrate Q, normalized by the reference volume flowrate for the single phase flow Q_{SP}, for the viscosity stratified liquid-liquid flow at $Re_\tau = 100$ and different viscosity ratios λ: $\lambda = 1$, $\lambda = 0.875$ and $\lambda = 0.75$. The arrow points in the direction of decreasing λ (i.e. increasing of the viscosity difference between the two fluid layers).

is $dt = 1 \times 10^{-4}$. Further details on the numerical method can be found in [15,19,20].

The computational domain used in our simulations has dimensions $4\pi h \times 2\pi h \times 2h$ along the streamwise (x), spanwise (y) and wall-normal (z) directions, and is discretized using $512 \times 256 \times 257$ grid nodes. Periodicity is applied along x and y for both $\mathbf{u}$ and ϕ. In the wall normal direction (z), no slip conditions are enforced for $\mathbf{u}$, whereas a normal contact angle (and a zero-flux of the chemical potential) is used for ϕ.

Simulations are run at a reference Reynolds number $Re_\tau = 100$ (defined based on the physical properties of fluid 2, i.e. the thicker fluid layer), and at Weber number $We = 0.1$. Assuming that $\rho u_\tau^2 = 2$ and that $h = 0.02$ m, the corresponding value of the surface tension is $\sigma = 0.2$ N/m. Although this value of σ is substantially larger than that of actual crude oil ($\sigma \simeq 0.05$ N/m), we believe that present results can still be of help to understand the dynamics of the liquid-liquid mixture. [16]. Three different values of the viscosity ratio are chosen: $\lambda = 1$, $\lambda = 0.875$ and $\lambda = 0.75$. This means that the viscosity of the thin fluid layer (fluid 1) is lower than the reference viscosity of the thick fluid layer (fluid 2). The value of Ch and Pe numbers comes from a combined physical-numerical consideration. For immiscible fluids, the interface thickness is of the order of molecular length scales, hence $Ch \to 0$. This would require a numerical resolution that is far beyond current computational possibilities. For this reason, we set $Ch = 0.02$, which guarantees that the interface between the two fluids is described using a minimum of 3 points in each direction. Then we assumed $Pe \propto Ch^{-1}$ to obtain a correct evaluation of the interface dynamics [without interface deterioration, see 16, and references therein]. In the present case, we chose $Pe = 150$, which minimizes the mass leakage (always below 2%).

4. Results

Simulations are run starting from a single phase turbulent flow at $Re_\tau = 100$. The order parameter ϕ is initialized such that the interface is initially flat and locate at $h_1/h_2 = 1/9$ (close to the upper boundary). The development of the two-phase flow at three different values of the viscosity ratio $\lambda = 1$, $\lambda = 0.875$ and $\lambda = 0.75$ is studied. Turbulence adjusts to the new physical configuration (transient behaviour) and finally reaches a new statistically steady state condition, after which results are collected for a time window long enough to ensure statistical convergence of the results.

We start our analysis by looking at the time evolution of the mean volume flowrate Q of the thicker fluid layer (fluid 2) across the channel section. Results, which are shown in Fig. 2, are normalized by the reference volume flowrate for the single phase case (Q_{SP}) at the same reference Re_τ ($Re_\tau = 100$). Here time is in wall units, $t^+ = t^* u_\tau^2/\nu_2$ (with t^* the physical time expressed in seconds). We clearly observe that, even for $\lambda = 1$, the presence of a deformable interface (characterized by a specific surface tension) separating the two fluid layers induces an overall increase of the volume flowrate (up to $\simeq$ 4%). This indicates that the wall normal transport of momentum is reduced, with a significant proportion of the mean flow energy being lost into interface deformation. For reducing λ, the volume flowrate further increases (up to $\simeq$ 10% for $\lambda = 0.75$). This is a direct consequence of the presence of a thin liquid layer with lower viscosity that reduces the mean shear stress at the upper wall. Since our simulations are run with an imposed pressure gradient, reducing the wall stress produces an increase of the mean volume flowrate. The explicit computation of the wall shear stress for the different simulations (at both the bottom and the top wall), as well as the corresponding value of the mean volume flowrate Q/Q_{SP}, is summarized in Table 1.

Table 1
Measurements of the shear stress at the bottom wall $\tau_{w,2}$ and the top wall $\tau_{w,1}$ for the different flow configurations ($\lambda = 1$, $\lambda = 0.875$ and $\lambda = 0.75$). Results from the single phase simulation (SP) are also shown. The value of the dimensionless volume flowrate Q/Q_{SP} corresponding to each specific simulation is also shown.

Simulations	$\tau_{w,2}$	$\tau_{w,1}$	Q/Q_{SP}
SP (Single Phase)	1	1	1
$\lambda = 1$	1.267	0.763	1.035
$\lambda = 0.875$	1.281	0.722	1.062
$\lambda = 0.75$	1.314	0.683	1.093

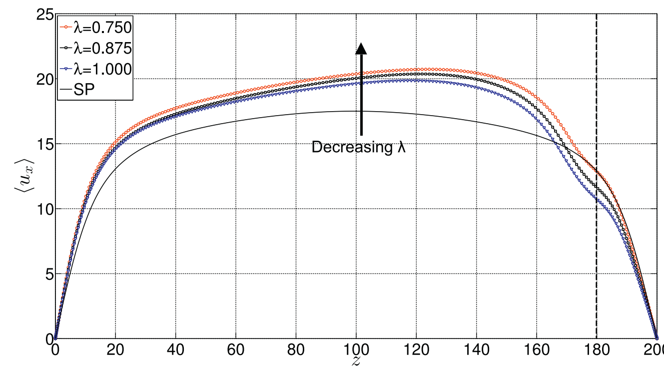

Fig. 3. Mean fluid streamwise velocity $\langle u_x \rangle$ for the viscosity stratified liquid-liquid flow at $Re_\tau = 100$. Comparison between simulations at different viscosity ratios λ: $\lambda = 1$ ($-\triangledown-$), $\lambda = 0.875$ ($-\square-$) and $\lambda = 0.75$ ($-\bigcirc-$). Results from simulation of single phase flow at the same reference shear Reynolds number (SP, -) are also included for comparison.

Linked to the observed changes of the volume flowrate, we expect large modification of the mean streamwise velocity. In Fig. 3 we explicitly show the wall-normal behavior of the mean streamwise velocity $\langle u_x \rangle$ for the three different values of λ considered in this study ($\lambda = 1, \lambda = 0.875, \lambda = 0.75$). The wall-normal coordinate is expressed in wall units, $z^+ = z^* u_\tau/\nu$ (with z^* the physical position expressed in meters). In the following, the superscript + will be dropped for ease of notation. Angular brackets $\langle\cdot\rangle$ denote averaging in time and over the homogeneous directions. Note that the reference position of the interface is explicitly shown by the thick vertical line. Statistics in this figure, as well as in the following figures, are averaged over a time window of $\Delta t^+ = 2000$, after a steady state condition is reached (as visible in Fig. 2 for $t^+ > 3000$). Where explicitly shown, arrows inside figures point in

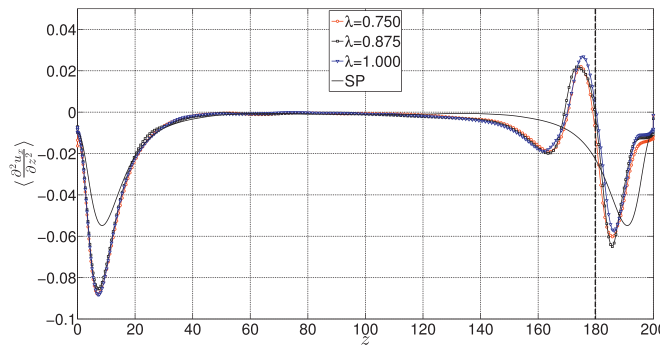

Fig. 4. Curvature of the mean fluid streamwise velocity, $\partial^2\langle u_x\rangle/\partial z^2$ for the viscosity stratified liquid-liquid flow at $Re_\tau = 100$. Lines as in Fig. 3.

the direction of decreasing λ (i.e. increasing the viscosity difference between the two fluid layers).

Compared to the reference case of a single phase flow (-), the presence of two different fluid layers separated by a deformable interface alters the symmetry of the profile: larger values of the velocity characterize the thick fluid layer ($0 < z < 180$), whereas smaller values of the velocity characterize the thin fluid layer ($180 < z < 200$). The lower is the viscosity of the thin layer in contact with the upper wall (i.e. the lower is λ), the larger are the values of the mean streamwise velocity. This is consistent with the observed behavior of Q/Q_{SP} (Fig. 2) and indicates that the presence of two different fluid layers separated by a deformable interface suppresses the wall-normal transport of momentum compared to the case of a single phase flow at the same Re_τ. The suppression of wall-normal momentum transport is the consequence of the conversion of kinetic energy into work to deform the liquid-liquid interface (potential energy). Although all the simulations are run with the same driving pressure gradient (i.e. with the same reference shear Reynolds number Re_τ), the presence of a deformable interface separating the two liquid layers alters the slope of the mean velocity at the wall (i.e. alters the viscous wall stress). The presence of a viscosity difference between the two layers ($\lambda \neq 1$) alters further the symmetry of the profile. The lower is λ, (i.e. the lower the viscosity of the thin layer), the larger is the mean velocity, since the rate of change of $\langle u_x\rangle$ with z is directly linked to the local value of the viscosity.

It is interesting to note that the mean streamwise velocity $\langle u_x\rangle$ presents an inflection point at the location of the interface. This is explicitly demonstrated in Fig. 4 by looking at the curvature of the mean streamwise velocity profile, $\partial^2\langle u_x\rangle/\partial z^2$. Differently from the case of a single phase flow where the curvature is always negative, for the liquid-liquid flow the curvature of the profile is always negative but in a thin region close to the fluid-fluid interface ($170 < z < 180$), where it becomes positive (i.e. change of curvature). This behavior is primarily due to the shear exerted by the layers at the interface and will be further analyzed below within the discussion of turbulence fluctuations.

To analyze the effect of the viscosity stratification on the behavior of turbulence, we compute the root mean square (rms) of the streamwise, spanwise and wall-normal fluid velocity fluctuations as a function of the wall normal coordinate z. Results are shown in Fig. 5. We will consider first the behavior of $\langle u'_{x,rms}\rangle$, panel a) in Fig. 5. Regardless of the value of λ, we clearly see that velocity fluctuations are only slightly modified (increased) near the lower wall ($0 < z^+ < 100$), where typical near wall-turbulence is maintained.

The situation remarkably changes near the top wall ($100 < z^+ < 200$). A first comparison is made between results from the single phase flow (solid line, -) and results from the two-phase flow at

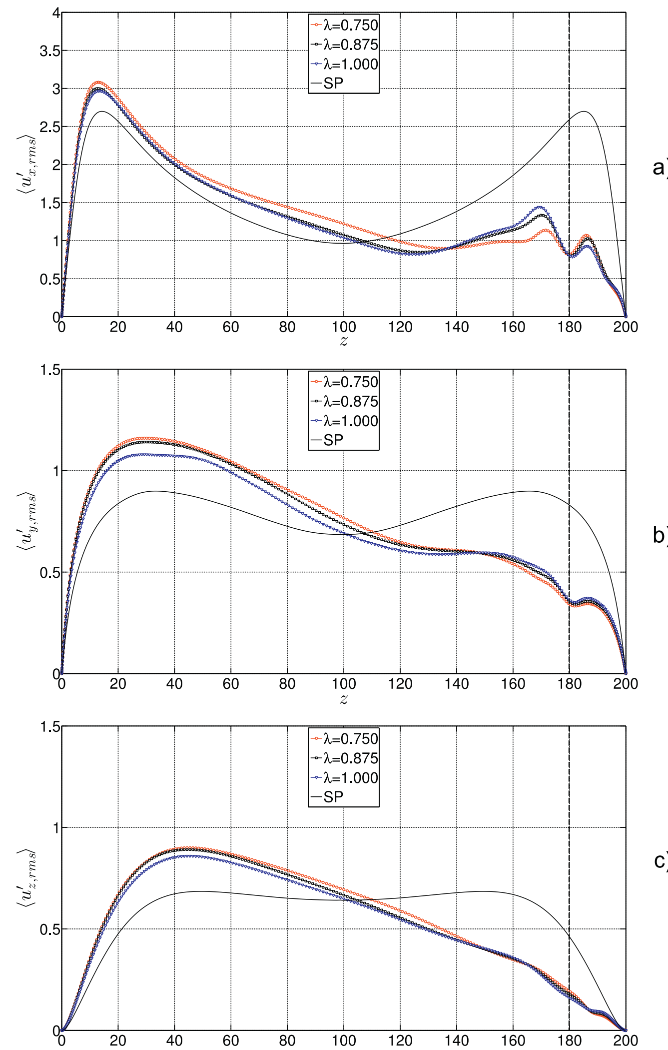

Fig. 5. Root mean square of fluid velocity fluctuations, $\langle u'_{i,rms}\rangle$, for the viscosity stratified liquid-liquid flow at $Re_\tau = 100$: a) streamwise component, $\langle u'_{x,rms}\rangle$; b) spanwise component, $\langle u'_{y,rms}\rangle$, c) wall-normal component, $\langle u'_{z,rms}\rangle$. Lines as in Fig. 3.

$\lambda = 1$ (symbols, $-\nabla-$). Turbulence is substantially suppressed compared to the case of a single phase flow, since in that region of the channel the deformable interface converts the kinetic energy of the mean flow into potential energy (interface deformation). Note that a local minimum of $\langle u'_{x,rms}\rangle$ is observed when approaching the location of the interface ($z^+ \simeq 180$). The effect of decreasing λ is particularly pronounced in the proximity of the interface ($140 < z^+ < 190$) and is twofold: it decreases turbulence fluctuations in the thin layer with lower viscosity ($180 < z^+ < 190$) while decreasing it in the thick layer with larger viscosity. A link can be drawn between the behavior of the turbulent fluctuations in the streamwise direction and the behavior of the mean flow strain rate $\gamma_{xz} = \partial\langle u_x\rangle/\partial z$, which is shown in Fig. 6. As far as the mean strain rate γ_{xz} is concerned, the behavior in the single phase flow (- in Fig. 6) is well known: $|\gamma_{xz}|$ decreases sharply in the near wall regions while attaining an almost constant value $|\gamma_{xz}| \simeq 0$ in the core of the channel. Compared to the single phase flow, for the case of the viscosity stratified liquid-liquid layer $|\gamma_{xz}|$ is increased near the bottom wall ($z^+ = 0$) and decreased near the top wall ($z^+ = 200$). From a vis-a-vis analysis of $\langle u'_{x,rms}\rangle$ and γ_{xz} we can infer the following: larger strain rates enhance the production of turbulent kinetic energy through the increase of the production term in the corresponding balance equation, whereas

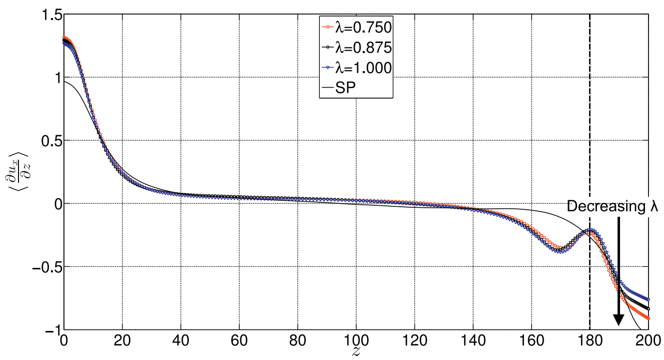

Fig. 6. Wall-normal behavior of the mean strain rate, $\gamma_{xz} = \partial \langle u_x \rangle / \partial z$ for the viscosity stratified liquid-liquid flow at $Re_\tau = 100$. Lines as in Fig. 3.

smaller strain rates reduce it. With similar arguments, we can also explain the behavior of $\langle u'_{x,rms} \rangle$ for different λ. In the thin liquid layer, for decreasing λ we observe an increase of $|\partial \langle u_x \rangle / \partial z|$, which is in turn associated to an increase of turbulence fluctuations. By contrast, when crossing the interface into liquid layer 2, $|\partial \langle u_x \rangle / \partial z|$ decreases for decreasing λ, which corresponds to a decrease of turbulent fluctuations.

For completeness, we also compute the behavior of spanwise ($\langle u'_{y,rms} \rangle$, Fig. 5b) and wall normal velocity fluctuations ($\langle u'_{z,rms} \rangle$, Fig. 5c). A decrease of turbulence intensities is observed for both $\langle u'_{y,rms} \rangle$ and $\langle u'_{z,rms} \rangle$ in the liquid-liquid interface region (near the upper wall, for $z > 120$). This finding agrees with the observation that the presence of the interface reduces the transport of momentum (in particular in the wall-normal direction) by converting the kinetic energy of the flow into potential energy (interface deformation). In the meantime, turbulence intensities are increased near the bottom wall, as a consequence of the increased shear rate therein (see Fig. 6 and related comments). Note that the shape of the $\langle u'_{y,rms} \rangle$ and $\langle u'_{z,rms} \rangle$ profiles for different λ is qualitatively similar, although a clear increase of turbulence fluctuations is observed near the lower wall for decreasing λ (as explicitly shown in Fig. 5).

We conclude our analysis on turbulence modulation in viscosity stratified liquid-liquid flow by computing the spanwise vorticity $\omega_y = \partial u_z / \partial x - \partial u_x / \partial z$, whose behavior is intimately linked to that of γ_{xz} just described. Instantaneous maps of ω_y for the different cases considered in this work are shown in Fig. 7. For the single phase flow (panel a), the vorticity distribution is almost symmetric and is characterized by long streaky structures emitted from both the bottom and top walls and reaching the core of the channel. In the case of viscosity stratified liquid-liquid layers with equal ($\lambda = 1$, Fig. 7b) or different viscosity ($\lambda \neq 1$, Fig. 7c–d), the flow symmetry is lost. In particular, turbulence is promoted far from the interface (near the bottom wall in Fig. 7), while it is reduced close to the interface (near the top wall in Fig. 7). Interestingly, we note the production of counterotating rolls induced by the shear at the liquid-liquid interface (black patches attached at the liquid-liquid interface). Their size and strength depends primarily on the surface tension at the interface and on the value of λ, with the intensity of the rolls decreasing with decreasing λ due to the reduced interfacial friction.

5. Conclusions

In this work, we used Direct Numerical Simulation to analyze the turbulent Poiseuille flow of two immiscible liquid layers inside a flat channel. The two fluid layers were characterized by the same density but different viscosity. In particular, a thin layer with smaller viscosity (fluid 1) moved on top of a thick layer with larger viscosity (fluid 2). The thickness ratio between the two liquid layers was $h_1/h_2 = 1/9$. Simulations, based on a Phase Field (PF) method to describe the interaction between the two liquid layers, were run at a reference shear Reynolds number $Re_\tau = 100$. Three different values of the viscosity ratio $\lambda = \nu_1/\nu_2$ between the two liquid layers were considered: $\lambda = 1$, $\lambda = 0.875$ and $\lambda = 0.75$.

Compared to the single phase flow, the presence of a liquid-liquid interface altered significantly the overall fluid dynamics of the system. Regardless of the value of λ, the volume flowrate across the channel section increased, indicating a significant turbulence reduction due to the conversion of the mean kinetic energy into potential energy at the deformed liquid-liquid interface (work is spent to deform the interface). These effects increased for decreasing λ. Future developments include the extension of presents results to a larger range of viscosity ratio.

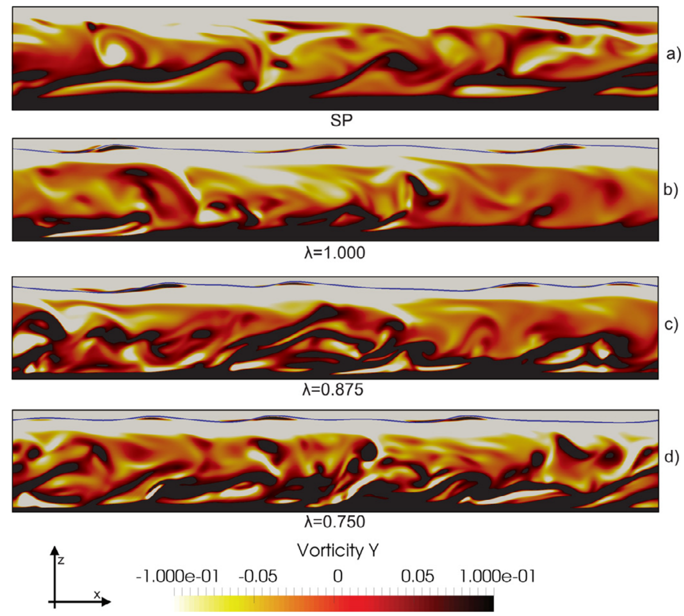

Fig. 7. Contour maps of the spanwise vorticity $\langle \omega_y \rangle$ for the viscosity stratified liquid-liquid flow at $Re_\tau = 100$ and different viscosity ratio λ. Panels: a) Single Phase flow; b) liquid-liquid flow at $\lambda = 1$; c) liquid-liquid flow at $\lambda = 0.875$; d) liquid-liquid flow at $\lambda = 0.75$. The location of the interface is explicitly indicated (thin black line) for clarity.

Acknowledgements

Support from EU FP7 Nugenia-Plus project (grant agreement No. 604965) and from Regione Autonoma Friuli Venezia Giulia under grant PAR FSC 2007/2013 is gratefully acknowledged. CINECA Supercomputing Centre (Bologna, Italy), SISSA (Trieste, Italy) and VSC (Vienna Scientific Cluster, Vienna) are also gratefully acknowledged for generous allowance of computer resources.

References

[1] Yiantsios SG, Higgins BG. Linear stability of plane poiseuille flow of two superposed fluids. Phys Fluids 1988;31:3225–38.
[2] Su YY, Khomami B. Numerical solution of eigenvalue problems using spectral techniques. J Comput Phys 1992;100:297–305.
[3] Blennerhassett PJ. On the generation of waves by wind. Philos Trans R Soc London Series A 1980;298:451–94.
[4] Renardy M, Renardy Y. Derivation of amplitude equations and the analysis of sideband instabilities in two-layer flows. Phys Fluids A 1993;5:2738–62.
[5] Lin M, Moeng C, Tsai W, Sullivan PP, Belcher SE. Direct numerical simulation of wind-wave generation processes. J Fluid Mech 2008;616:1–30.
[6] Zonta F, Soldati A, Onorato M. Growth and spectra of gravity–capillary waves in countercurrent air/water turbulent flow. J Fluid Mech 2015;777:245–59.
[7] Kao TW, Park C. Experimental investigations of the stability of channel flows. part 2. two-layered co-current flow in a rectangular channel. J Fluid Mech 1972;52:401–23.

[8] Joseph DD, Renardy M, Renardy Y. Instability of the flow of two immiscible liquids with different viscosities in a pipe. J Fluid Mech 1984;141:309–17.
[9] Hu HH, Lundgren TS, Joseph DD. Stability of core-annular flow with a small viscosity ratio. Phys Fluids A 1990;2(11):1945–54.
[10] Chen K, Bai R, Joseph DD. Lubricated pipelining. part 3 stability of core-annular flow in vertical pipes. J Fluid Mech 1990;214:251–86.
[11] Bai R, Chen K, Joseph DD. Lubricated pipelining: stability of core-annular flow. part 5. experiments and comparison with theory. J Fluid Mech 1992;240:97–132.
[12] Jacqmin D. Calculation of two-phase navier–stokes flows using phase-field modeling. J Comput Phys 1999;155(1):96–127.
[13] Yue P, Feng JJ, Liu C, Shen J. A diffuse-interface method for simulating two-phase flows of complex fluids. J Fluid Mech 2004;515:293–317.
[14] Badalassi VE, Ceniceros HD, Banerjee S. Computation of multiphase systems with phase field models. J Comput Phys 2003;190(2):371–97.
[15] Scarbolo L, Molin D, Perlekar P, Sbragaglia M, Soldati A, Toschi F. Unified framework for a side-by-side comparison of different multicomponent algorithms: lattice boltzmann vs. phase field model. J Comput Phys 2013;234:263–79.
[16] Scarbolo L, Bianco F, Soldati A. Coalescence and breakup of large droplets in turbulent channel flow. Phys Fluids 2015;27:073302.
[17] Kim J. Phase-field models for multi-component fluid flows. Commun Comput Phys 2012;12(3):613–61.
[18] Zheng X, Babaee H, Dong S, Chryssostomidis C, Karniadakis G. A phase-field method for 3D simulation of two-phase heat transfer. Int J Heat Mass Transf 2015;82:282–98.
[19] Zonta F, Marchioli C, Soldati A. Modulation of turbulence in forced convection by temperature-dependent viscosity. J Fluid Mech 2012a;697:150–74.
[20] Zonta F, Onorato M, Soldati A. Turbulence and internal waves in stably-stratified channel flow with temperature-dependent fluid properties. J Fluid Mech 2012b;697:175–203.